RESILIENT INFRASTRUCTURE
June 1–4, 2016

BEHAVIOR OF GFRP-REINFORCED CONCRETE SQUAT WALLS UNDER SIMULATED EARTHQUAKE LOADING

Ahmed Arafa
PhD student, Université de Sherbrooke, Canada

Ahmed Sabry Farghaly
Postdoctoral fellow, Université de Sherbrooke, Canada

Brahim Benmokrane
Professor, Université de Sherbrooke, Canada
NSERC Research Chair in FRP Reinforcement for Concrete Infrastructure
Tier-1 Canada Research Chair in Advanced Composite Materials for Civil Structures

ABSTRACT

Steel-reinforced squat walls are used as the main component for earthquake resistance in low-rise structures. Deterioration due to corrosion of steel reinforcement is one of the major challenges facing the construction industry. Furthermore, given the low aspect ratio of squat walls, their behavior is dominated by inelastic shear deformations activated by the yielding of flexural reinforcement. These deformations degrade strength and stiffness with subsequent shear failure, preventing the wall from achieving its flexural capacity, which is a prerequisite for adequate seismic design. Using noncorrodible glass-fiber-reinforced-polymer (GFRP) bars represents an effective method for overcoming corrosion problems. In addition, the available experimental studies on mid-rise shear walls show that GFRP reinforcement can control shear deformation, which is a major problem with steel-reinforced squat walls. Our study was experimentally conducted to investigate the shear-deformation behavior of GFRP-reinforced squat walls. Two full-scale squat walls with an aspect ratio of 1.3 were constructed and tested to failure under quasi-static reversed cyclic lateral loading: one was reinforced with steel bars; the other with GFRP bars. The experimental results show that the GFRP-reinforced wall evidenced significantly enhanced behavior related to ultimate strength, drift ratio, control shear distortion, and mode of failure compared to the steel-reinforced wall.

Keywords: Squat walls; Concrete; GFRP; Shear distortion; Seismic.

1. INTRODUCTION

Squat walls are defined as structural walls with an aspect ratio (h_w/l_w; h_w: wall height and l_w: wall length) less than 2.0. This type of wall is widely used as the primary seismic-force resisting component in low-rise structures such as nuclear facilities and industrial buildings. Moreover, such walls also frequently serve as bridge piers and abutments (Salonikios 2007). Because of their low aspect ratios, squat walls—unlike slender walls—generate high shear forces at their bases to develop structural flexural strength, which makes shear capacity a major issue in their design (Paulay et al.1982; Kuang and Ho. 2008; Whyte and Stojadinovic. 2014). Experimental investigations have demonstrated that the behavior of squat walls is dominated by inelastic shear deformations, indicating that these deformations develop and significantly increase with the onset of flexural-reinforcement yielding (Saatcioglu. 1991; Sittipunt et al. 2001; Massone et al. 2009; Takahashi et al. 2013). These deformations, in turn, rapidly degrade strength and stiffness with subsequent shear failure.

Using fiber-reinforced-polymer (FRP) bars as the main reinforcement in concrete structures in harsh environments is becoming a widely accepted solution in overcoming the problem of steel corrosion (ACI Committee 440 2007). Due to the relatively lower cost of glass-FRP (GFRP) bars compared to the other commercially available FRP bars, the

use of GFRP bars in reinforced concrete (RC) structures has found their way into numerous applications such as bridge deck slabs, beams, and columns (El-Salakawy et al. 2005; Kassem et al. 2011, Tobbi et al. 2014).
Recently, and under the demand of constructing a multistory building with adequate strength and stiffness using GFRP reinforcement, an experimental study was conducted by Mohamed et al. (2014) to investigate the validity of using GFRP bars in reinforcing mid-rise shear walls to resist lateral loads. The reported test results clearly revealed that properly designed and detailed GFRP-reinforced walls could reach their flexural capacities with no strength degradation with a reasonable deformability in inelastic stage. It was also found that using elastic materials (GFRP bars) distributed the shear strain along the wall height; resulting in control the shear deformation than those experienced in steel-reinforced shear wall, in which the yielding of the flexural reinforcement caused localization of shear deformation at the yielding zone.

As a continuation, an extensive experimental study is under way to investigate the feasibility of GFRP-reinforced concrete squat walls with different configuration and details. This paper reports only one GFRP-reinforced squat wall and its counterpart steel-reinforced one to evaluate the behavior of such structural element under quasi-static reversed cyclic lateral loading. The investigation focused on assessing failure modes, ultimate capacity, and hysteretic response.

2. EXPERIMENTAL PROGRAM

2.1 Specimen Design

Two full-scale squat walls were constructed and tested under quasi-static reversed cyclic lateral loading up to failure. The first specimen, SX4, was reinforced with conventional steel bars, while the second specimen, GX4, was reinforced with GFRP bars. The walls were designed according to the minimum requirement of CSA A23.3 (2014) and CSA S806 (2012). The specimens measured 1500 mm in length, 2000 mm in height, and 200 mm in thickness, resulting in an aspect ratio of 1.30, which classifies them as squat walls according to CSA codes. Each specimen was cast with a rigid base to serve as anchorage for the vertical reinforcement and to enable the test specimens to be fastened to the laboratory's testing floor (Figure 1a).

The two specimens were reinforced with the same reinforcement ratio and configuration. Two boundary elements of eight #3 (steel or GFRP) bars of equal length and width (200 × 200 mm) were placed at each end of the horizontal dimension. The longitudinal reinforcement in the boundaries were laterally tied against premature buckling with #3 transverse-reinforcement spiral ties (steel or GFRP) spaced at 80 mm along the total wall height. Two layers of horizontal and vertical web reinforcement were used. The horizontal web reinforcement consisted of #4 bars (steel or GFRP) spaced at 80 mm, while the vertical web reinforcement consisted of #3 bars (steel or GFRP) spaced at 120 mm. Figure 1b and Table 1 shows the reinforcement details.

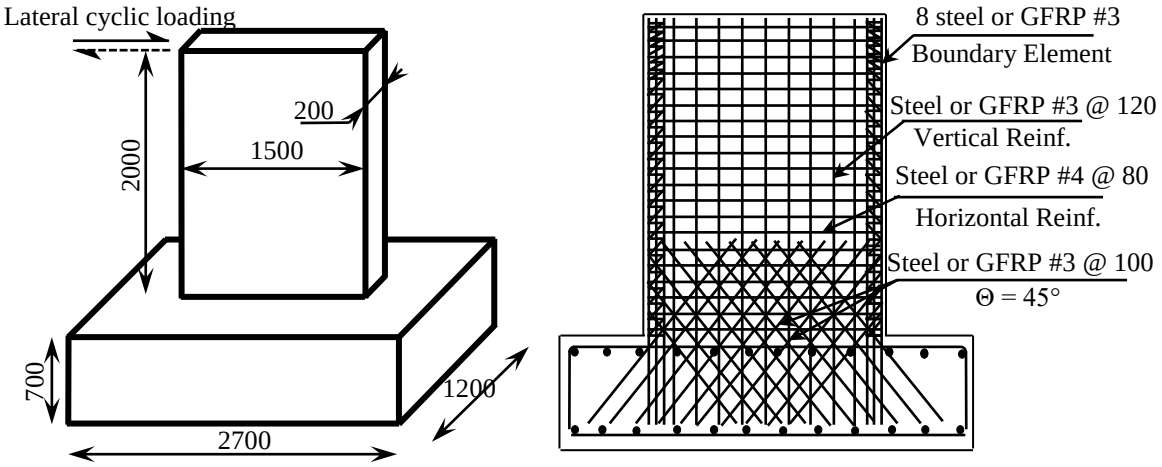

a) Concrete dimensions b) Reinforcement

Figure 1: Details of specimens

The GFRP-reinforced wall, GX4, was designed to have nearly equal flexural capacity and shear capacity. Plane sectional analysis was carried out to predict the ultimate flexural capacity, considering the unconfined (0.0035 concrete compressive strain for both walls) and confined concrete (0.005 and 0.007 concrete compressive strain for SX4 and GX4, respectively [Paulay and Preistly (1995); Mohamed et al. 2014]). The analysis was based on strain compatibility, internal force equilibrium, and the controlling mode of failure. Regarding the shear capacity, owing to the absence of seismic provisions for GFRP-reinforced squat walls in the CSA S806 (2012), the concept provided in CSA A23.3 (2014) for steel was used. The horizontal web reinforcement was calculated—according to CSA S806 (2012)—to carry all shear forces associated with the development of flexural capacity, as no reliance should be placed on the concrete in contributing to shear strength in the case of large cracks associated with flexural failure. Sliding shear was prevented between the wall specimen and the rigid base by adding two layers of cross-diagonal #3 GFRP bars at an angle of 45° spaced at 100 mm and sufficiently anchored on each side of the shear plane (Figure 1b). The anchorage length for both the vertical reinforcement and cross-diagonal sliding reinforcement was equal to the development length specified in CSA S806 (2012) multiplied by 1.25 to account for the cyclic effect, as suggested by Mohamed et al. (2014). Since the steel-reinforced squat wall, SX4, served as a reference for GX4, the reinforcement configuration and ratio was identical in both specimens. Table 1 lists the predicted flexural and shear strength for the tested specimens. The material reduction and safety factors in the design equations used in this study were set equal to unity, since the material strengths and specimen dimensions were known.

Table 1 - Reinforcement details and calculated capacities of the walls

Wall	f_c'	Reinforcement Ratio					P_u (kN)	V_r (kN)	Unconfined		Confined	
		ρ_l	ρ_t	ρ_v	ρ_h	ρ_s			V_{func} (kN)	P_u/V_{func}	V_{fcon} (kN)	P_u/V_{fcon}
SX4	34.8	1.43	0.89	0.59	1.58	0.48	534	1548	549	0.97	630	0.85
GX4	40.4			0.59	1.58	0.48	912	895	764	1.30	995	0.92

f_c' = concrete compressive strength; ρ_l = boundary longitudinal-bar reinforcement ratio; ρ_t = boundary-tie reinforcement ratio; ρ_v = web vertical-bar reinforcement ratio; ρ_h = web horizontal-bar reinforcement ratio; ρs = diagonal sliding shear reinforcement ratio; P_u = experimental ultimate lateral load; V_r = predicted shear capacity; V_{func} = predicted flexural capacity with unconfined concrete; V_{fcon}= predicted flexural capacity with confined concrete.

2.2 Material Properties

The test specimens were cast using normal-weight, ready-mixed concrete with a target 28-day compressive strength of 40 MPa. The actual concrete compressive strength (f_c') was determined based on the average of at least three 100 × 200 mm cylinders for each specimen on the day of specimen testing. Table 1 presents the actual concrete strengths of the test specimens.

Table 2 - Mechanical properties of the reinforcement

Bar	d_b (mm)	A_f (mm^2)	E_f (GPa)	f_{fu} (MPa)	ε_{fu} (%)
Straight bars					
#3 GFRP	9.5	71	65	1372	2.11
#3 steel	9.5	71	200	f_y = 420	ε_y = 0.2
#4 steel	12.7	129	200	f_y= 420	ε_y = 0.2
Bent GFRP bars					
#3 GFRP	Straight portion	50	1065	2.1	
	Bent portion	---	460	---	
#4 GFRP	Straight portion	50	1020	2.0	
	Bent portion	---	459	---	

d_b: bar nominal diameter, A_f: nominal cross-sectional area, E_f: modulus of elasticity, f_{fu}: guaranteed tensile strength, εfu: ultimate strain, f_y: steel yielding strength, ε_y: steel yielding strain.

Two types of reinforcing bars were used in this study: grade 400 deformed steel bars and GFRP bars. The GFRP bars were sand-coated, and made of continuous boron free glass fibers impregnated in a thermosetting vinyl-ester resin. The tensile properties of the GFRP bars were determined by testing five specimens according to ASTM D7205 (ASTM 2011) for straight bars. Test method B.5 in ACI 440.3R (2004) was used to determine the tensile properties of the bent bars. The tensile properties of the steel bars were provided by the manufacturer. Table 2 lists all the mechanical properties of the reinforcement used in this study.

2.3 Instrumentation

A series of strain gauges and linear variable displacement transducers (LVDTs) were used to monitor the deformation response of the test specimens. One LVDT was mounted at the top of the squat wall to measure the lateral displacement. One LVDT was installed at the construction joint between the wall and the base to monitor sliding between the wall and base. Two LVDTs were mounted at the boundary elements to measure concrete strain. For stability, two additional LVDTs were attached to the upper steel beam to measure unlikely out-of-plane deformation. The crack width was also measured with two LVDTs mounted at the first two major cracks.

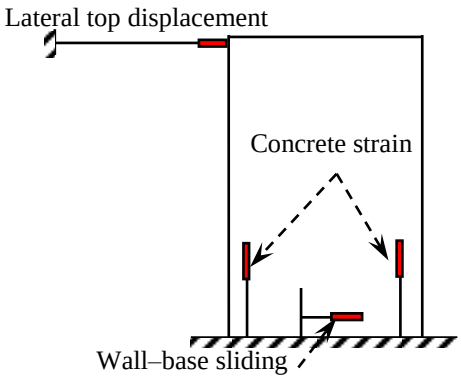

Figure 2: Instrumentation

2.4 Test Setup and Procedure

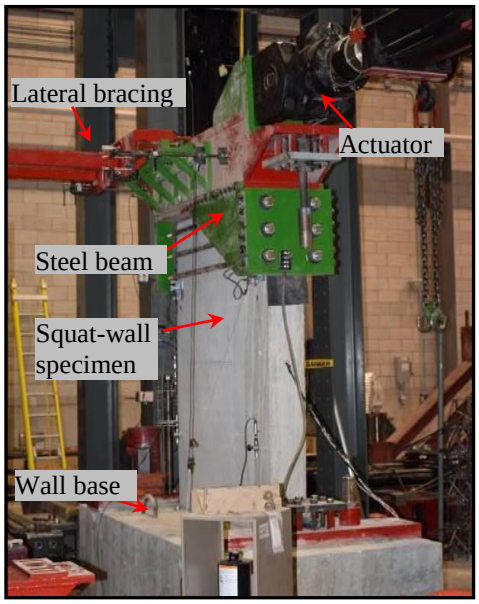

Figure 3: Test setup of the wall specimens

Figure 3 shows the test setup. The specimens were tested laterally as a vertical cantilever with forces applied through a specially fabricated steel load-transfer assembly; no axial load was applied to any of the test specimens as it is the critical shear case of the squat walls emphasizing that no post seismic axial capacity was evaluated for the

tested walls. Lateral loading was applied with a 1000 kN MTS-hydraulic actuator. Out-of-plane bracing was provided at the level of transfer steel beam to prevent the wall specimen from twisting during testing.

Lateral loading was applied to the specimens in several steps under displacement-control mode throughout the test. Each loading step consisted of two identical displacement cycles in increments of ±2 mm up to 10 mm, followed by increments of ±5 mm drift up to 50 mm, and thereafter increments of ±10 mm up to failure. Figure 4 presents a typical sequence of the displacement cycles.

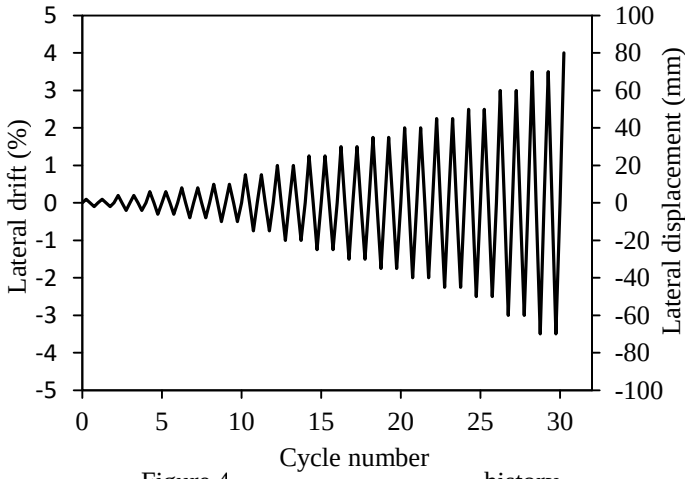

Figure 4. Applied displacement history

3. TEST RESULTS AND OBSERVATIONS

3.1 General Behavior and Modes of Failure

Figure 5 depicts the typical crack propagation for the tested walls. The first initial cracks propagated at the lower part of the walls at a load of 175 kN (33% of ultimate load), and 164 kN (18% of ultimate load), and with initial crack widths of 0.1 mm and 0.12 mm for specimens SX4 and GX4, respectively. These cracks were predominantly horizontal along the boundary elements and perpendicular to the direction of the maximum stress induced by the bending moment. Upon further loading, these cracks acquired some inclination in the central zone of the web, owing to shear stresses in this region.

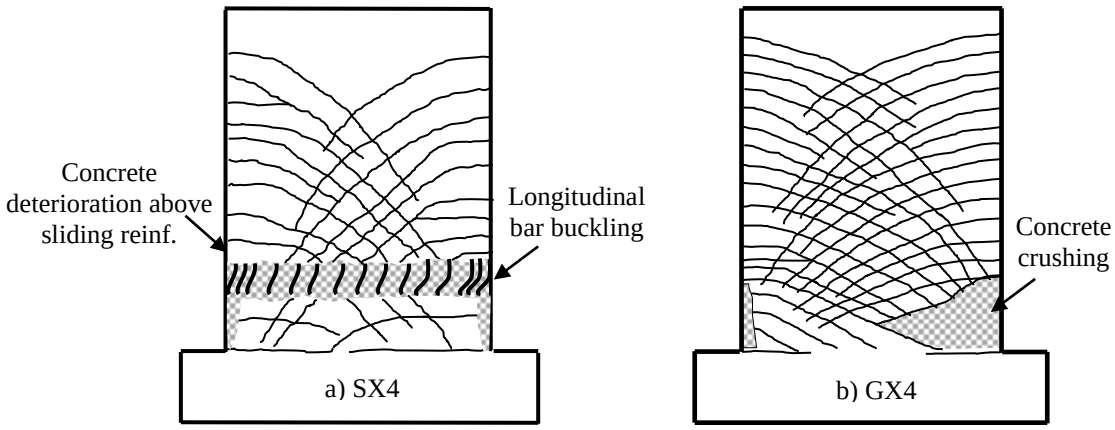

Figure 5: Crack pattern

As loading continued, horizontal cracks in the boundary elements accompanied by shear cracks at the web continued to propagate up to 1/3 of the wall height. With further increased displacement, new shear cracks tended to propagate closer to the top of the wall and extended over the wall height. Such cracks were steeper than those that propagated

in the lower part of the wall, although their inclination and width were significantly decreased close to the boundary element. This control stems from the presence of heavily reinforcement and confinement in the boundary elements, which are known to favorably affect the shear capacity of squat walls (Salonikios et al. 1999; Kassem. 2015). As larger displacements were applied, flexural-shear or shear cracks originating from one side continued to progressively extend down to the opposite boundary element with increased inclination, intersecting the cracks originating from the other side and forming crisscross pattern. It is clear that crack propagation was more distributed and intensive in GX4 than in SX4.

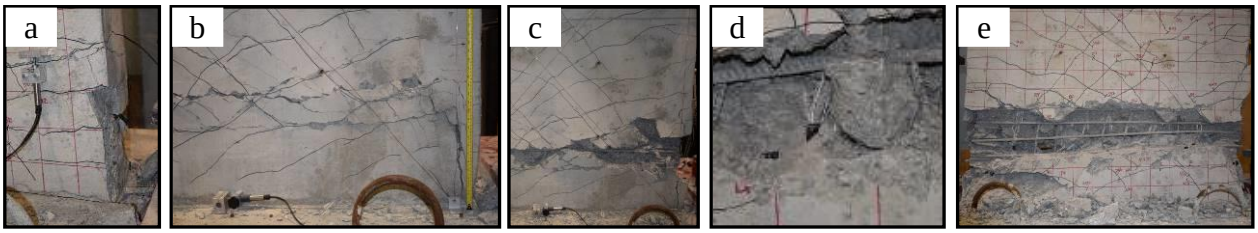

Figure 6: Failure progression of specimen SX4: (a) spalling of concrete cover; (b) concrete deterioration above sliding reinforcement; (c) spalling of the deteriorated concrete (d) buckling of longitudinal reinforcement causing failure; (e) specimen face at failure

With further displacement, spalling of the concrete cover became more significant at the most compressed ends of the walls at lateral drift of 1.25% and 1.75% for specimen SX4 and GX4, respectively (as shown in Figures 6a, and 7a for specimens SX4 and GX4, respectively). At this stage, yielding of longitudinal reinforcement in SX4 became significant and localized at the plastic-hinge zone, which extended over a height of approximately 2.5 times the wall thickness (510 mm) and was just above the diagonal cross sliding reinforcement. As a result, localized shear deformations in SX4 accompanied by excessive deterioration of the concrete cover along this region was clearly evidenced at a lateral drift ratio of 1.5%, as shown in Figure 6b. More deterioration of the concrete and sequential spalling along this zone was observed during subsequent cycles, producing a progressive degradation in lateral strength (Figure 6c). When loading was continued to push SX4 to 2.0% drift, a substantial deteriorated zone above the cross sliding reinforcement associated with in-plane buckling of boundary longitudinal bars and vertical web reinforcement formed (Figure 6d), leading to failure, since this stage was followed by drastic drop in the lateral strength during reversed loading. Figure 6e shows the specimen at the end of testing. It should be mentioned that, due to the additional shear resistance provided by the diagonal cross sliding reinforcement, the most damaged wall section was pushed away from the base–wall interface, where the interaction between moment and shear is the largest.

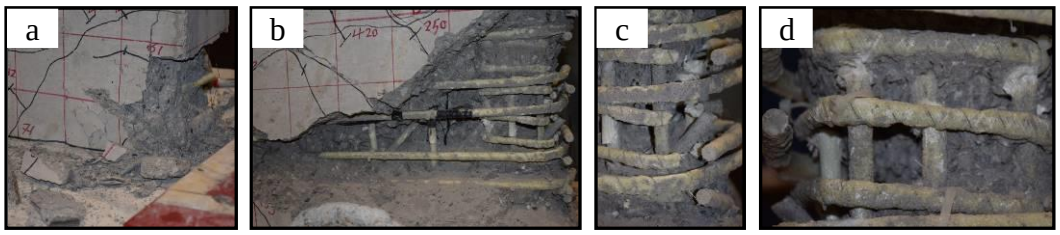

Figure 7: Failure progression of specimen GX4: (a) spalling of concrete cover; (b) concrete crushing causing failure; (c) rupture of GFRP ties; (d) fracture of compressed longitudinal bars

In the case of GX4, the specimen continued carrying loads in each cycle with no strength degradation. The specimen's failure was gradual, starting with gradual deterioration and splitting of concrete in the compressed boundary element at 2.6% drift. More noise was generated from the compressed zone, and it was much easier to judge that flexural failure was imminent. The specimen ultimately failed at a drift ratio of 3.0% in flexural compression (Figure 7b) associated with rupture at the bent portion of the GFRP ties (Figure 7c) and fracture in the compressed longitudinal bars (Figure 7d).

It is interesting that the test observations revealed that the formed cracks in the GX4 tended to realign and almost close between load reversals (at zero loading) with negligible residual crack widths up to a lateral drift of 1.75% (corresponding to concrete-cover spalling). In contrast, the residual crack width in SX4 was significant, especially after yielding of the longitudinal steel reinforcement. This observation is attributed to the elastic nature of the GFRP bars and could be considered as an advantage in using GFRP bars and provide evidence of satisfactory bond between the GFRP bars and concrete. Furthermore, the test results show that SX4 exhibited smaller crack widths at the early stages of loading than did GX4. After the yielding point, however, the crack widths substantially increased and become remarkably larger than that in GX4; the measured maximum crack widths at failure were 6 mm and 2.1 mm for SX4, and GX4, respectively. Additionally, although the same reinforcement ratios and configurations have been utilized in both specimens, SX4 exhibited extensive shear deformations accompanied by deterioration of concrete and followed by buckling of the longitudinal bars though the maximum applied shear force is much smaller than the shear strength computed according to CSA A23.3 (2014), while the failure of GX4 was generated by flexural compression and the full flexural capacity for confined section was achieved as will be discussed. Furthermore, the shear deformation in SX4 was clearly localized at the plastic hinge zone causing the extensive concrete deterioration leading to the premature failure; meanwhile, due to the elastic behavior of the GFRP bars, GX4 experienced distributed shear deformation along the wall height.

Furthermore, no sign for distress due to sliding shear was observed in SX4 and GX4, since the measured sliding displacement at the wall–base interface was negligible (1% of the total displacement). The main reason for this is the effect of using cross diagonal sliding reinforcement which controlled the potential sliding crack between the wall and base and subsequently promoting all components of sliding shear resistance mechanisms; shear friction maintained by aggregate interlock and tensile resistance of the cross diagonal sliding reinforcement to work collectively to resist sliding deformations which have been reported in many researches that have detrimental effect in the behavior of squat walls and should be avoided (Paulay et al 1982; Salonikios et al. 1999; Whyte and Stojadinovic. 2014).

3.2 Hysteretic Response

Figure 8 depict the hysteretic response of SX4 and GX4. In addition, the points at which different types of physical damage occurring during cyclic loading are plotted to give a visual reference of the relationship between hysteretic response and damage progress in the tested specimens.

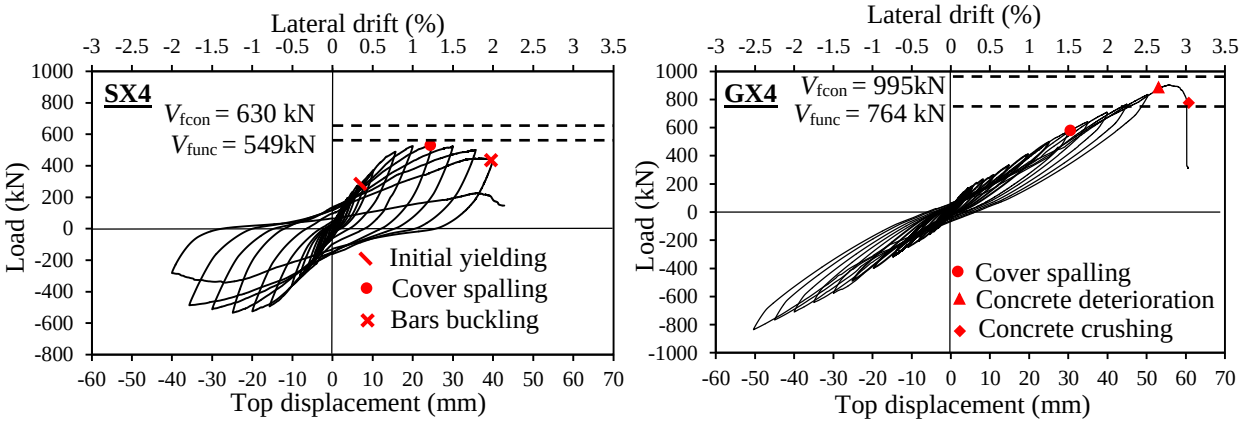

Figure 8: Hysteretic response

SX4 has an initial linear branch corresponding to the uncracked condition of the wall. At a lateral drift ratio of 0.18% (176 kN), the first crack propagated and reduced wall stiffness. Yielding of the longitudinal reinforcement at the boundary elements occurred at a drift ratio of 0.4% (309 kN), followed by opening in the hysteretic loops and a gradual decrease in overall stiffness. As the lateral drift increased, the hysteretic loops gradually increased, accompanied by larger residual displacement. After unloading in one direction, reloading in the opposite direction met low initial resistance until the previously opened shear cracks closed. As the cracks closed, the walls started to gradually recover their strength. The specimen achieved its ultimate capacity of 534 kN at the first cycle on drift ratio of 1.25% and then this capacity started to decrease. Once the specimen experienced buckling in the

longitudinal reinforcement at boundary elements at the first cycle of lateral drift ratio of 2.0%, the corresponding lateral strength was 82% of the peak load and was followed by lateral strength in the negative direction of 52% of the peak load. It should be mentioned that, even though the specimen was properly confined at the boundary elements, the experimentally obtained capacity was almost equal to the predicted flexural capacity for the unconfined concrete (549 kN). The main reason for this is the localized shear deformations, which prevented the walls from achieving their flexural capacity.

On the other hand, the response of GX4 was essentially linear-elastic up to 0.2% drift (164 kN) at which a slight reduction in stiffness induced by the propagation of the first crack was observed. As loading progressed, gradual degradation in overall stiffness was observed that can be attributed to the evolution of crack propagation. The unloading/reloading curves appear to demonstrate linearity as a result of the linear–elastic behavior of the GFRP bars. In addition, the reloading branches followed a similar loading path but at a lower loading stiffness resulting in lower peak strength. By increasing loading up to a drift ratio of 1.75% (572 kN), the crack propagation stabilized and the concrete cover at the most compressed end spalled. As a result, the hysteretic loops began to open in a manner suggesting the onset of inelastic behavior in the wall. This was also observed in mid-rise shear walls tested by Mohamed et al. (2014). Indeed, after this stage, the specimen lost self-centering ability, similar to that observed by Mohamed et al. (2014). The specimen continued withstand loading without strength degradation up to 2.6% drift (859 kN) which corresponds to concrete deterioration through cover splitting in the compressed zone. Thereafter, the specimen exhibited an insignificant increase in load with increasing displacement up to 2.75% drift corresponding to the ultimate load of 912 kN. This was followed by gradual strength degradation to 88% of the peak capacity as displacement progressed up to 3.0% drift. This capacity then suddenly dropped due to concrete crushing. It is of interest to note that the maximum measured capacity is similar to the predicted flexural capacity for confined-concrete, as listed in Table 1. This bears out the recommendation made by Mohamed et al. (2014) that well-detailed lateral-resisting walls reinforced with GFRP bars can achieve their flexural capacity with no strength degradation, which is the primary requirement in lateral-resisting elements.

The hysteresis response, depicted in Figure 8, shows that, due to the low modulus of elasticity of the GFRP bars, GX4 exhibited a softer hysteretic response than SX4 up to 1.3% drift (intersecting point of the two envelope curves, corresponding to 99% and 56% of ultimate load for SX4 and GX4, respectively). After that point, SX4 exhibited significant deterioration in strength up to failure at 2% lateral drift, while GX4 kept increasing almost linearly to failure at 3%, achieving a 71% higher capacity than it steel counterpart. It should be noted that the CSA A23.3 (2014) requires that the structural walls should be able to maintain its structural integrity and at least three-quarters of its ultimate capacity through peak displacements equal to a story drift ratio of 2.0%. Although this drift ratio was achieved in both specimens, the fact that GX4 achieved larger ultimate drift and capacity could be considered as GFRP-reinforced squat walls providing higher safety margins in the event of an earthquake.

3.3 Energy Dissipation

Energy-dissipation capacity is usually used to assess the seismic response of reinforced-concrete members as it can be used as a response indicator in the design of short-period structures and structures subjected to a long-duration earthquake. Although the accumulative dissipated energy when the structure fails is an important parameter, it does not clearly indicate the level of deformation at which this energy is dissipated. On the other hand, the amount of energy dissipated at a given drift level allows for more meaningful comparisons between different structures, yet it has to be supplemented by an indicator of the structure's residual force; if not, the picture is rather incomplete (Mohamed et al 2014).

Figure 9-a shows the calculated accumulative dissipated energy at each cycle for the tested squat walls. For drifts lower than 1%, the dissipated energy was quite small. For larger drifts, however, a nearly linear increase of the dissipated energy with respect to an increase in drift level can be observed. SX4 had higher dissipated energy than GX4. It is interesting to note that both walls experienced similar energy dissipation (31 and 28 kN.m, respectively) at lateral drifts of 1.25 and 2%, respectively, corresponding to cover spalling, which is considered moderate damage (CSA A23.3 2014 and NRC 2010). As the lateral load increased, SX4 experienced higher inelastic deformation than GX4, yielding to higher dissipated energy in comparison to GX4.
In order to compare the effectiveness of the dissipated energy for the two walls, residual displacement (remaining displacement at zero force) was plotted against the accumulated energy dissipated in each cycle (Figure 9-b). It is

clearly shows that the energy dissipation of SX4 was accumulated due to the high residual displacement, while GX4 exhibited minimal residual displacement due to the capability of self-centering behavior of GFRP-reinforced walls.

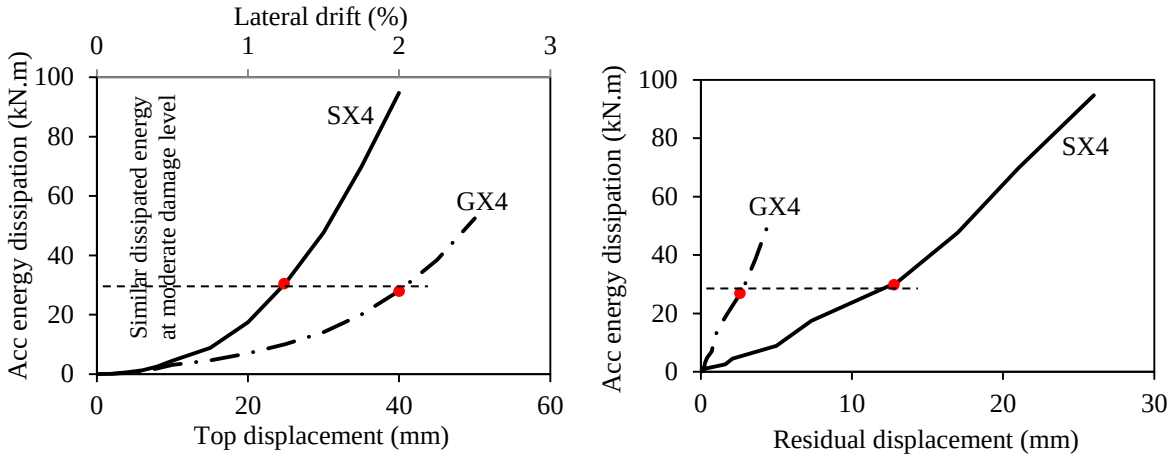

Figure 9: Energy Dissipation

Clearly, SX4 achieved higher energy dissipation than GX4 in each loop with substantial residual displacement due to the inelastic nature and Bauschinger effect of steel reinforcement after yielding. Due to the absence of a yielding point in the GFRP bars, GX4 exhibited linear-elastic behavior with insignificant residual deformations. This means that the GFRP-reinforced wall will require minimal repair after earthquake ground-shaking events, while the steel-reinforced wall will be technically difficult to repair as the result of excessive permanent displacements caused by concentrated wall damage with yielding in the plastic-hinge zone. As a result, rebuilding might be more economical than repairing. Garcia and Miranda (2005) reported that recent seismic events have highlighted the necessity of demolishing damaged structures due to excessive permanent deformations, even though they did not collapse.

4. CONCLUSIONS

An experimental study was carried out to evaluate the use of GFRP bars in reinforcing squat walls under seismic loading. Based on the experimental results, the following conclusions were reached:

- The shear deformation in SX4 was localized due to the extensive yielding of the longitudinal steel reinforcement, while the elastic behavior of the GFRP bars distributed the shear deformation over the wall height in GX4. This allowed the walls to gain their full flexural capacity with no signs of premature shear, sliding shear, bond or anchorage failure, or instability failure.
- The realignment and recoverable behavior of GX4 at up to 2% lateral drift (corresponding to the moderate damage) indicates that it would withstand seismic loading and require minimal repair. In contrast, SX4 exhibited substantial deformations at the same level of lateral drift.
- The GFRP ties at the boundary elements of GX4 were adequate to provide the required confinement. The experimentally obtained load was 28% higher than the predicted flexural capacity for the unconfined section.
- The GFRP-reinforced wall exhibited adequate warning through large splitting and deterioration of concrete under compression prior to failure.

ACKNOWLEDGEMENTS

The authors wish to acknowledge the financial support of the Natural Sciences and Engineering Research Council of Canada (NSERC), the Canada Research Chair in Advanced Composite Materials for Civil Structures, and the Fonds Quebecois de recherche – Nature et Technologies – (FQR-NT).

REFERENCES

ACI Committee 440 2004. Guide Test Methods for Fiber-Reinforced Polymers (FRPs) for Reinforcing or Strengthening Concrete Structures (ACI 440.3R-04). *American Concrete Institute*, Farmington Hills, MI, 40 pp.

ACI Committee 440 2007. Report on Fiber-Reinforced Polymer (FRP) Reinforcement Concrete Structures (ACI 440R-07). *American Concrete Institute*, Farmington Hills, MI, 100 pp.

CSA A23.3 2014. Design of Concrete Structures Standard. *Canadian Standards Association*, Mississauga, Ontario, Canada, 240 pp.

CSA S806 2012. Design and Construction of Building Components with Fiber-Reinforced Polymers. *Canadian Standards Association*, Mississauga, Ontario, Canada, 208 pp.

El-Salakawy, E., Benmokrane, B., El-Ragaby, A. and Nadeau, D. 2005. Field Investigation on the First Bridge Deck Slab Reinforced with Glass FRP Bars Constructed in Canada. *ASCE J. of Composites for Constr.*, 9 (6): 470-479.

Kassem, C., Farghaly, A. S. and Benmokrane, B. 2011. Evaluation of flexural behavior and serviceability performance of concrete beams reinforced with FRP Bars. *ASCE J. of Composites for Const.*, 15 (5), 682-695.

Kassem, W. 2015. Shear strength of squat walls: A Strut-and-Tie Model and Closed-Form Design Formula. *Engineering Structures*, 84: 430-438.

Kuang, J. S. and Ho, Y. B. 2008. Seismic Behavior and Ductility of Squat Reinforced Concrete Shear Walls with Nonseismic Detailing. *ACI Structural Journal*, 105 (2): 225-231.

Massone, L. M., Orakcal, K. and Wallace, J. W. 2009. Modeling of Squat Structural Walls Controlled by Shear. *ACI Structural Journal*, 106 (5): 646-655.

Mohamed, N., Farghaly, A. S., Benmokrane, B. and Neale, K. W. 2014. Experimental Investigation of Concrete Shear Walls Reinforced with Glass-Fiber-Reinforced Bars under Lateral Cyclic Loading. *ASCE Journal of Composites for Constructions*, 18 (3): 04014001.

National Research Council of Canada, NRC, 2010, Canadian commission on building and fire codes. *National Building Code of Canada* (NBC), Ottawa, 1167 pp.

Paulay T., and Priestley M. J. N. 1995. Seismic Design of Reinforced Concrete and Masonry Buildings. *John Wiley and Sons, Inc*.

Paulay, T., Priestley, M. J. N. and Synge, A. J. 1982. Ductility in Earthquake Resisting Squat Shear walls. *ACI Journal*, 79 (4): 257-269.

Razaqpur, A. G. and Isgor, O. B. 2006. Proposed Shear Design Method for FRP-Reinforced Concrete Members without Stirrups. *ACI Structural Journal*, 103 (1): 93-102.

Ruiz-García, J. and Miranda E. 2005. Performance-based assessment of existing structures accounting for residual displacements. Technical Report No. 153, The John A. Blume Earthquake Engrg Ctr, Stanford Univ., Calif.

Saatcioglu, M. 1991. Hysteretic Shear Response of Low-Rise Walls. *Proceedings of International Workshop on Concrete Shear in Earthquake*, The National Science Foundation, University of Houston, Texas, 105-114.

Salonikios, T. N., Kappos, A. J., Tegos, I. A. and Penelis, G. G. 1999. Cyclic Load Behavior of Low-Slenderness Reinforced Concrete Walls: Design Basis and Test Results. *ACI Structural Journal*, 96 (4): 649-660.

Salonikios, T. N. 2007. Analytical Prediction of the Inelastic Response of RC Walls with Low Aspect Ratio. *ASCE Journal of Structural Engineering*, 133 (6): 844- 854.

Sittipunt, C., Wood, S. L., Lukkunaprasit, P. and Pattararattanakul, P. 2001. Cyclic Behavior of Reinforced Concrete Structural Walls with Diagonal Web Reinforcement. *ACI Structural Journal*, 98 (4): 554-562.

Takahashi, S., Yoshida, K., Ichinose, T., Sanada, Y., Matsumoto, K., Fukuyama, H. and Suwada, H. 2013. Flexural Drift Capacity of Reinforced Concrete Wall with Limited Confinement. *ACI Structural Journal*, 110 (1): 95-104.

Tobbi, H., Farghaly, A. S. and Benmokrane, B. 2014. Behavior of Concentrically Loaded Fiber-Reinforced Polymer Reinforced Concrete Columns with Varying Reinforcement Types and Ratios. *ACI Structural Journal*, 111 (2): 375-386.

Whyte, C. and Stojadinovic, B. 2014. Effect of Ground Motion Sequence on Response of Squat Reinforced Concrete Shear Walls. *ASCE Journal of Structural Engineering*, 140 (8): 4014004.